Space-Time Adaptive Matched-Field Processing (STAMP)

Yung P. Lee
Science Applications International Corporation
1710 SAIC Drive, McLean, VA 22102
(Tel) 703-676-6512, (Fax) 703-893-8753

yung@osg.saic.com

ABSTRACT

In airborne or space-based radar systems for which the platform is in motion, the major land clutter exhibits a unique Doppler-azimuth slant-ridge distribution where land clutter is up-Doppler shifted in the forward azimuths and is down-Doppler shifted in the aft-ward azimuths. Similarly, reverberation received in mobile towed-array active sonar systems has the same Doppler-azimuth slant-ridge distribution. Space-time adaptive processing (STAP) is two-dimensional jointed filtering that adaptively suppresses clutter or reverberation to enable the detection of moving targets away from the clutter or reverberation ridge. In STAP, an sensor array provides spatial discrimination, while a sequence of time returns or pulses form a synthetic array provides Doppler (velocity) discrimination.

In passive sonar, long integration time is used to enhance narrowband signal detection against broadband ambient and/or interference background. Because of the complex multi-paths in shallow water environment, multi-paths of a signal propagating inside a conic angle might spread in wide azimuths (relative to a horizontal line array). Multi-paths in different azimuths propagate in different group speeds; long integration time will also resolve them in different Dopplers. The signal spread in Doppler-azimuth is most serious in the forward and aft-end-fire directions of a towed horizontal array. In forward end-fire, own-ship noise is inevitable and makes signal detection more difficult.

Matched-Field Processing (MFP) that uses a propagation code to predict the complex multi-paths and coherently combines them to provide range/depth discrimination has been studied and demonstrated extensively in the past two decades. MFP incorporating with an appropriate motion model has also been demonstrated to estimate the source velocity and localize source in range and depth [1]. The proposed STAMP processing combines the adjacent-filter beamspace post-Doppler STAP [2] and MFP to provide improved performance for mobile multi-line-towed-array sonar applications. The processing scheme includes: transforming phone time snapshots into the frequency domain, forming horizontal beams at each frequency bin in the directions of interest for each towed line, and combining signals from multi-towed-lines, adjacent Doppler bins and beams that cover the multi-path Doppler-azimuth spread due to motion using adaptive MFP. A simulation of STAMP performance in the towed-array forward-looking problem will be discussed

Paper presented at the RTO SET Symposium on "Capabilities of Acoustics in Air-Ground and Maritime Reconnaissance, Target Classification and Identification", held in Lerici, Italy, 26-28 April 2004, and published in RTO-MP-SET-079.

1. Introduction

Element-space pre-Doppler STAP [2] is two-dimensional fully adaptive processing that coherently combines the signals from the elements of an array and the multiple snapshots of coherent signals to obtain large spatial and temporal signal gain, suppress interference, and provide target detection in azimuth and velocity. Computational complexity and the need to estimate the interference from limited snapshots make it difficult for real-time implementation. A few cost effective algorithms having real-time capability are mentioned in [3]. The adjacent-filter beamspace post-Doppler STAP is a reduced-dimension partially adaptive approach. It performs a Doppler filtering with a temporal Fourier transform and a spatial filtering with the conventional beamforming before adaptive processing. The adaptive processing is done in a selected subspace including a few beams and a few Doppler bins [4].

In the complex multipath underwater environment, signals propagate along a vertical slice of ocean within a critical angle defined by the boundary condition of the local ocean environment. Because of the spread in vertical propagation angles, signals observed by a horizontal array will be spread into many horizontal beams when signals arrive off the broadside direction. In addition, signals that propagate in different vertical angles have different phase speeds. Thus when a source moves toward or away from the array it also spreads over many Dopplers if a long temporal integration time is used. Without combining the spread energy in beam and Doppler space, a processor will encounter severe signal mismatch and degradation. Space-time MFP that uses a propagation code to model the signal spread over beams and Dopplers and coherently combines them should provide improvement in signal estimation while simultaneously providing range and depth localization. Lee [1] demonstrated the single-element pre-Doppler space-time MFP with real passive sonar data in a shallow water environment. Klemm [5] introduced the element-space pre-Doppler space-time adaptive MFP and illustrated the principle with some numerical examples for active sonar. In this paper, the beam-space post-Doppler space-time adaptive MFP is presented and its performance with a multi-line tow array is studied through a passive sonar simulation.

This paper is organized as follows: Section 2 reviews the robust white-noise-constrained adaptive beamforming, Section 3 reviews the matched field processing, Section 4 shows a few examples of matched field processing with real data, Section 5 describes STAMP processing, Section 6 shows the simulation scenario and results for forward-sector processing, and Section 7 gives a summary of this study.

2. Wideband-Narrowband White-Noise-Constrained Method

Adaptive processing uses the measured signal plus noise data vectors to minimize the sidelobe contributions from those components that do not match with the steering vector for a given search cell. Let $\mathbf{R}$ be the covariance matrix of the received signal and noise, and $\mathbf{R}=\langle \mathbf{X}\mathbf{X}^{+} \rangle$ where $\langle\rangle$ denotes ensemble average over a number of sequential data vectors $\mathbf{X}$ and "+" denotes Hermitian transpose. The minimum variance distortionless response (MVDR) method minimizes the variance at the output of a linear weighting of the hydrophone array subject to the distortionless constraint that signals in the "look direction" have unity gain. The formulation minimizes the variance given by

$$S_{MVDR} = \mathbf{W}^{+}\mathbf{R}\,\mathbf{W}$$

with respect to the weighting $\mathbf{W}$, subject to the unity gain constraint

$$\mathbf{W}^{+}\mathbf{A} = 1$$

where $\mathbf{A}$ is a steering vector. The MVDR weight vector $\mathbf{W}_{MVDR}$ can be derived as

$$\mathbf{W}_{MVDR} = \frac{\mathbf{R}^{-1}\mathbf{A}}{\mathbf{A}^{+}\mathbf{R}^{-1}\mathbf{A}}$$

where $\mathbf{R}^{-1}$ is matrix inversion. The MVDR output is

$$S_{MVDR} = \frac{1}{\mathbf{A}^{+}\mathbf{R}^{-1}\mathbf{A}}$$

Applying the singular-value decomposition method, the covariance matrix $\mathbf{R}$ can be decomposed into a set of eigenvectors $\mathbf{V}_n$ associated with a set of eigenvalues λ_n,

$$\mathbf{R} = \sum_{n=1}^{N} \lambda_n \mathbf{V}_n \mathbf{V}_n^{+}$$

and the inverse of the covariance matrix is given by

$$\mathbf{R}^{-1} = \sum_{n=1}^{N} \frac{1}{\lambda_n} \mathbf{V}_n \mathbf{V}_n^{+}$$

The MVDR weight vector becomes

$$\mathbf{W}_{MVDR} = \frac{\sum_{n=1}^{N} \frac{1}{\lambda_n} \left(\mathbf{V}_n^{+}\mathbf{A}\right)\mathbf{V}_n}{\sum_{n=1}^{N} \frac{1}{\lambda_n} \left|\mathbf{V}_n^{+}\mathbf{A}\right|^2}$$

The MVDR output becomes

$$S_{MVDR} = \left(\sum_{n=1}^{N} \frac{1}{\lambda_n} \left|\mathbf{V}_n^{+}\mathbf{A}\right|^2 \right)^{-1}$$

Without mismatch between data and model and when the signal is loud enough, the steering vector $\mathbf{A}$ is perfectly matched with signal eigenvector in the "look direction". The rest of eigenvectors are orthogonal to the steering vector and have no effect on the output. But, when mismatch is present, the steering vector is no longer orthogonal to the rest of eigenvectors. The noise vectors associated with the least significant eigenvalues then dominate the inverse processing and degrade the signal estimation.

All forms of mismatch are either deterministic or random. Deterministic mismatch degrades the signal estimation and causes localization bias, but it can be minimized if more prior knowledge is included in modeling the signal. Random mismatch degrades the signal estimation but will not bias the localization. Random mismatch cannot be minimized so that robust algorithms were developed to tolerate a certain level of random mismatch. The white-noise-gain constrained (WNC) method referred to Cox [11], dynamically adjusts the sensor noise level by adding white noise power to the diagonal elements of the covariance matrix subject to an inequality constraint on the sensor noise gain. This technique is called LSMI (loaded sample matrix inverse) in the radar community. Adding noise expands the noise space and effectively eliminates small eigenvalues that would otherwise dominate the sum in the MVDR output calculation due to mismatch.

The MVDR white noise processing gain, defined as the amplitude squared of the weight vector $\left|\mathbf{w}_{MVDR}\right|^2$, is directly proportional to the signal-to-noise ratio (SNR). The MVDR signal degradation due to mismatch is

inversely proportional to the SNR. At low SNR, the white noise processing gain approaches unity (the conventional linear processing noise gain) and the mismatch effect is negligible. At high SNR, the white noise processing gain is high and the MVDR output is very sensitive to mismatch. For each steering direction, the WNC method dynamically adjusts the sensor noise level by adding white noise to the diagonal elements of the covariance matrix. Adding white noise lowers the "apparent" SNR so that the processing becomes less sensitive to mismatch. Adding white noise, in the amount ε, to the diagonal elements of the covariance matrix is the same as adding ε to each eigenvalues without modifying the eigenvectors. The WNC weight vector $\mathbf{w}_{WNC}$ that result is

$$\mathbf{W}_{WNC} = \frac{(\mathbf{R}+\varepsilon)^{-1}\mathbf{A}}{\mathbf{A}^{+}(\mathbf{R}+\varepsilon)^{-1}\mathbf{A}}$$

or

$$\mathbf{W}_{WNC} = \frac{\sum_{n=1}^{N}\frac{1}{\lambda_n+\varepsilon}\left(\mathbf{V}_n{}^{+}\mathbf{A}\right)\mathbf{V}_n}{\sum_{n=1}^{N}\frac{1}{\lambda_n+\varepsilon}\left|\mathbf{V}_n{}^{+}\mathbf{A}\right|^2}$$

and the WNC output is

$$S_{WNC} = \frac{\mathbf{A}^{+}(\mathbf{R}+\varepsilon)^{-1}\mathbf{R}(\mathbf{R}+\varepsilon)^{-1}\mathbf{A}}{\left|\mathbf{A}^{+}(\mathbf{R}+\varepsilon)^{-1}\mathbf{A}\right|^2}$$

or

$$S_{WNC} = \frac{\sum_{n=1}^{N}\frac{\lambda_n}{(\lambda_n+\varepsilon)^2}\left|\mathbf{V}_n{}^{+}\mathbf{A}\right|^2}{\left(\sum_{n=1}^{N}\frac{1}{\lambda_n+\varepsilon}\left|\mathbf{V}_n{}^{+}\mathbf{A}\right|^2\right)^2}$$

In this study a wideband-narrowband (WB/NB) implementation of the WNC method is used. WB/NB means using signal and noise in several adjacent frequency bins to form a wideband covariance matrix for adaptive weight vector estimation then applying the estimated weight to calculate narrowband response at each frequency bin. Instead of ensemble average data vectors over a sequence of time snapshots, averaging over a finite frequency band forms a wideband covariance matrix. For each steering direction, the MVDR white noise processing gain $\left|\mathbf{W}_{MVDR}\right|^2$ and the MVDR output are calculated. If the white noise processing gain falls below a pre-selected constraining value δ^2, the WNC weight vector is set equal to the MVDR weight. If the white noise processing gain is above the constraining value, an amount of white noise that equals the MVDR output is added in the processing and a new white noise processing gain $\left|\mathbf{W}_{WNC}\right|^2$ and a new output S_{WNC} are calculated. The new white noise processing gain then is compared with the constraining value. The process is repeated until the new white noise processing gain falls below the constraining value. The feedback-loop approach insures that the amount of white noise added in each iteration is adequate so that the iteration procedure converges rapidly without overshooting. The calculated adaptive weight then is used to filter data

vectors at each frequency bin. After filtering through all frequencies of interest, the maximum response over the frequencies is reported.

3. Matched Field Processing (MFP)

MFP refers to array processing algorithms that exploit the multipath structure of signals propagating in an ocean waveguide by using an acoustic model to calculate replica (steering) vectors in a search space. Measured signal plus noise data vectors are matched with the replica vectors and an ambiguity surface is computed. The locations at which peaks are found in the ambiguity surface are estimates of the source location. An excellent overview of MFP can be found in the paper by Baggeroer, et. al. [6].

In a slowly range varying environment, the adiabatic normal mode method [7] has proved to be effective in modeling sound propagation in an ocean waveguide. In a complex range dependent environment, the Parabolic Equation (PE) [8] marching algorithm has proved to be more accurate than the adiabatic normal mode method. Both of them are narrowband algorithms. The PE marching algorithm nominally uses a range step and a depth grid that is proportional to the wavelength. It becomes computationally intensive for increasing center frequency, range, and bandwidth. A recent work using the Gaussian beam Bellhop [9] ray trace method has shown promise in speeding up broadband range dependent propagation modeling. A book by F. B. Jensen et. al. [10] provides an excellent overview of these models.

In this study a shallow water range independent environment is assumed and the normal mode method is used to model signal propagation. The complex pressure at receiver location $\mathbf{r}$ and depth z due to a narrow-band source at range $\mathbf{r}_s$, depth z_s, and frequency w, can be expressed as

$$p(\mathbf{r},z;\mathbf{r}_s,z_s) = a\sqrt{2\pi}\sum_{m=1}^{M}\frac{\varphi_m(z)\varphi_m(z_s)}{\sqrt{k_m|\mathbf{r}_s-\mathbf{r}|}}e^{ik_m|\mathbf{r}_s-\mathbf{r}|}$$

where $m=1,.....,M$ are mode indices, $\varphi_m(z)$ are modal depth eigen-functions, k_m are modal horizontal wave numbers, and a is the narrow-band source amplitude. The depth eigen-functions and horizontal wave numbers satisfy:

$$\frac{d^2\varphi_m}{dz^2}+[k_0(z)^2-k_m{}^2]\varphi_m=0$$

where $k_0(z)=w/c(z)$ and $c(z)$ is the sound speed profile that covers the water column and extends into the sediment and ocean basement. The pressure field at a N-hydrophone receiving array can be modeled in a vector form as

$$\mathbf{P}^+(\mathbf{r}_s,z_s)=[p^*(\mathbf{r}_1,z_1;\mathbf{r}_s,z_s),p^*(\mathbf{r}_2,z_2;\mathbf{r}_s,z_s),.....p^*(\mathbf{r}_N,z_N;\mathbf{r}_s,z_s)]$$

where $(\mathbf{r}_i,z_i)$, $i=1,....,N$ are hydrophone locations. For a given search location $(\mathbf{r}_s,z_s)$, the MFP replica then is calculated as

$$\mathbf{A}(\mathbf{r}_s,z_s)=\mathbf{P}(\mathbf{r}_s,z_s)/\left|\mathbf{P}(\mathbf{r}_s,z_s)\right|$$

Let

$$\mathbf{X}^+=[x^*(\mathbf{r}_1,z_1),x^*(\mathbf{r}_2,z_2),.....,x^*(\mathbf{r}_N,z_N)]$$

be a data vector, a measured pressure field at the receiving array. The conventional MFP response at search location ($\mathbf{r}_s$,z_s) is calculated as

$$S_{CMFP}(\mathbf{r}_s, z_s) = \mathbf{A}^{+}(\mathbf{r}_s, z_s)\mathbf{X}$$

4. MFP Examples

MFP detects and localizes signals by exploiting multi-path structure of signals propagating in an ocean waveguide. One way to sample the multi-path signal structure within a short integration time is using a vertical array to exploit the depth diversity of the signal. In a shallow water experiment that took place in the northeastern Gulf of Mexico in November 1995, a vertical array was deployed and a source was towed along a 188-m depth bathymetry contour. The test area was located approximately 90 miles south of Panama City, Florida. Figure 1 shows a measured sound speed profile in the test area.

For the data presented here, the source broadcast a CW tone at 197 Hz towed at 76 m depth toward the array starting at approximately 9 km. The tow speed was approximately 2.5 m/s. Figure 2 shows a snapshot of the received and the predicted pressure fields when source was at 9.06 km. The predicted pressure field was calculated with a range-independent normal mode code. A complex multi-path interference structure versus depth is seen in Figure 2. MFP exploits this multipath interference structure to discriminate signal in range and depth. Figure 3 shows the resulting conventional MFP range-depth ambiguity surface. A peak appears at 9.06 km in range and 76 m in depth that is the estimated source location.

Another way to sample the multi-path signal structure is to exploit the range diversity of the signal. For arrays that do not have extended vertical aperture, MFP with a synthetic aperture was introduced [1,3]. Figure 4 shows the received and the predicted pressure fields on the bottom hydrophone for the same experiment over a period of 418-s. Within this extended period the source moved toward the receiver a distance of 1.063 km. The pressure field on the bottom hydrophone shows significant multi-path interference verse range. The data were sampled at 1.22 Hz so that Figure 4 could represent the pressure field observed on a 512-element synthetic horizontal array (HLA) whose aft-endfire toward the source. The synthetic HLA MFP, single-element pre-Doppler space-time MFP, uses this range varying multi-path structure to detect and localize source. The resulting conventional range-depth ambiguity surface for a synthetic HLA with spacing of 2.076 m (tow speed of 2.5 m/s toward receiver) is shown in Figure 5. Successful source localization of the single-element pre-Doppler space-time MFP is demonstrated. In this processing, source speed (the synthetic HLA spacing) is also a search parameter. Figure 6 shows the resulting conventional range-speed ambiguity surface for source depth of 76 m. The source range and speed are determined and the processing is sensitive to the search speed.

5. Space-Time Adaptive Matched Field Processing (STAMP)

Figure 7 shows the STAMP processing diagram for a multi-line tow array. It starts with Doppler processing, Fourier transformation of received hydrophone time series $x_{kl}(t)$ into frequency domain $X_{kl}(f)$,

$$X_{kl}(f) = FFT\{x_{kl}(t)\}$$

where l =1,…,L is the line index and k =1,…,K is the phone index in a line. A plane wave conventional beamforming response $b_l(f,\theta)$,

$$b_l(f,\theta) = \frac{1}{\mathrm{K}} \sum_{k=1}^{\mathrm{K}} X_{kl}(f) e^{i2\pi f(k-1)d\sin(\theta)/c}$$

is then calculated at each frequency bin for each towed line, where d is the hydrophone spacing and c is sound speed. A beam-space vector $\mathbf{B}(f_1,\theta_1)$,

$$\begin{aligned}\mathbf{B}(f_1,\theta_1) = [\ & b_1(f_1,\theta_1), b_1(f_1,\theta_1+\Delta\theta),\ldots,b_1(f_1,\theta_1+\mathrm{N}\Delta\theta),\\ & \ldots\ldots,\\ & b_1(f_1+\mathrm{M}\Delta f,\theta_1), b_1(f_1+\mathrm{M}\Delta f,\theta_1+\Delta\theta),\ldots,b_1(f_1+\mathrm{M}\Delta f,\theta_1+\mathrm{N}\Delta\theta),\\ & b_2(f_1,\theta_1), b_2(f_1,\theta_1+\Delta\theta),\ldots,b_2(f_1,\theta_1+\mathrm{N}\Delta\theta),\\ & \ldots\ldots,\\ & b_2(f_1+\mathrm{M}\Delta f,\theta_1), b_2(f_1+\mathrm{M}\Delta f,\theta_1+\Delta\theta),\ldots,b_2(f_1+\mathrm{M}\Delta f,\theta_1+\mathrm{N}\Delta\theta),\\ & \ldots\ldots,\\ & \ldots\ldots,\\ & b_{\mathrm{L}}(f_1,\theta_1), b_{\mathrm{L}}(f_1,\theta_1+\Delta\theta),\ldots,b_{\mathrm{L}}(f_1,\theta_1+\mathrm{N}\Delta\theta),\\ & \ldots\ldots,\\ & b_{\mathrm{L}}(f_1+\mathrm{M}\Delta f,\theta_1), b_{\mathrm{L}}(f_1+\mathrm{M}\Delta f,\theta_1+\Delta\theta),\ldots,b_{\mathrm{L}}(f_1+\mathrm{M}\Delta f,\theta_1+\mathrm{N}\Delta\theta)\ ]\end{aligned}$$

is formed with beam responses from all towed lines for selected beams from θ_1 to $\theta_1+\mathrm{N}\Delta\theta$ and Doppler bins from f_1 to $f_1+\mathrm{M}\Delta f$. The covariance matrix $\mathbf{R}$ is formed by the outer product of $\mathbf{B}(f_1,\theta_1)$ and ensemble averaged over a wide Doppler band.

$$\mathbf{R} = \left\langle \mathbf{B}(f_1,\theta_1)\mathbf{B}^{+}(f_1,\theta_1) \right\rangle_{f_1}$$

For MFP, predicted hydrophone pressure time series $p_{kl}(t)$ for a signal at search range $\mathbf{r}_s$, depth z_s, and relative speed v_s at frequency f_1 and bearing θ_1 are calculated with a propagation code for a known array shape and acoustic environment. They are then passed through the Doppler processing and the conventional beamforming, and are normalized to form the beam-space steering vector. The adaptive weight vector is calculated with the beam-space steering vector and the wideband (averaged over wide Doppler band) covariance matrix $\mathbf{R}$, then applied on each $\mathbf{B}(f_1,\theta_1)$ to get the adaptive narrowband response. It is noted that STAMP is the same as STAP when one replaces the propagation code with a plane-wave signal model.

6. Forward-Sector Processing Simulation Geometry

Figure 8 shows the simulation geometry of forward-sector processing. In this simulation, the tow ship noise and its bottom bounce energy are treated as stationary broadband point-interference. The target is 10 km in front of the tow ship at 90 m in depth. It broadcasts a narrowband signal and moves toward the tow ship with a relative speed of 6 kts. Three array configurations were considered: single-Line, 4-Line-Sequential, and 4-Line-vertical. Each single-Line consists of 48 phones with a spacing of 2.25 m. The arrays are at a nominal depth of 90 m. The 4-Line-Sequential configuration connects four single-lines to form a long horizontal line. The 4-Line-Vertical configuration stacks 4 single-lines vertically with a vertical spacing of 10 m. The environment used in this simulation is the same as the one described in section 4.

The conventional plane-wave beamforming of a single-Line, Figures 9 and 10 show beam/time responses (BTRs) and Doppler/Azimuth responses of each signal component, respectively. The own-ship and the bottom interference arrive at relatively higher angles away from the forward endfire at 0^{o}. The target component is buried underneath the own-ship interference in the combined BTR, but with 256-sec integration time, it begins to separate from own-ship noise in the Doppler/Azimuth response. The narrowband target

signal is spread in Doppler and azimuth due to multi-paths shown in Figure 10 that can be coherently combined with STAMP processing to enhance detection and localization. This is the motivation of the STAMP processing.

The top two panels in Figure 11 show the plane-wave beam spectrograms for single-Line steered at 10^o off the forward endfire. The high-angle own-ship noise leaks into this shallow angle and causes the high noise background in the conventional beam spectrogram, but is significant suppressed by the adaptive processing. The bottom left panel shows the STAMP track-cell-gram that tracks the target location and the bottom right panel shows the maximum response over Doppler. The STAMP uses beams of 0^o to 30^o and 6 Doppler bins for 6-kt search. It is noted that STAMP processing provides 2-3 dB more signal gain than the plane-wave processing for single-Line and provides 8-9 dB more with 4-Line-Vertical array.

Figure 12 shows the range tracking performance of the STAMP. In the simulation the target starts at 10 km and moves toward the towed ship. With single-Line, the conventional MFP does not provide range discrimination of the target. With adaptive MFP, single-Line STAMP starts to show the target track that is closing in range. The 4-Line configurations help to suppress the range sidelobes, and the 4-Line-Vertical array provides a better performance than the 4-Line-Sequential array.

Figure 13 shows depth discrimination of STAMP range tracking with the 4-Line-Vertical array. The target track is formed only at the target depth of 90 meters. The target-related cascaded sidelobes are seen at other depths. Similarly, Figure 14 shows speed discrimination of STAMP range tracking with the 4-Line-Vertical array. The target track is formed at the target speed of 3 m/s. Away from the target speed, the track becomes defocused and only target-related cascaded sidelobes are seen at search speeds far away from the target speed.

7. Summary

STAMP processing that combines STAP and MFP has been developed. Simulations show that STAMP coherently combines signal multi-path spread in azimuth and Doppler and greatly enhances the target detection as well as providing target range and depth classification and localization. In future studies, the robustness of STAMP against array shape error, frequency mismatch, and environmental mismatch as well as how STAMP performs in other tactical scenarios will be addressed.

Reference:

[1] “Synthetic aperture matched-field processing,” Y. P. Lee, JASA 100, pp2851 (1996).
[2] “Space-Time Adaptive Processing for Airborne Radar,” J. Ward, Lincoln Laboratory Technical Report TR-1015, December 13, 1994.
[3] “*Principles of Space-Time Adaptive Processing”* R. Klemm, IEE, UK, 2002 Chapter 7.
[4] “On adaptive spatial-temporal processing for airborne surveillance radar systems,” H. Wang and L. Cai, IEEE Trans. AES, Vol. 30, No. 3, pp. 660-670, July 1994.
[5] “Interrelation between matched-field processing and airborne MTI radar,” R. Klemm, IEEE J. of Oceanic Eng., vol. 18, no. 3, pp. 168-180, July 1993.
[6] “An Overview of Matched Field Methods in Ocean Acoustics,” A. B. Baggeroer, W. A. Kuperman, and P. N. Mikhalevsky, IEEE J. of Oceanic Eng., vol. 18, no. 4, pp. 401-424, October 1993.
[7] “The KRAKEN normal mode program,” SACLANT Undersea Research Center Memorandum (SM-245)/Naval Research Laboratory Mem. Rep. 6920, 1991.
[8] “A split-step Pade solution for parabolic equation method,” M. D. Collins, J, Acoust. Soc. Am. Vol. 93, no. 4, pp. 1736-1742, April 1993.
[9] “Gaussian beam tracing for computing ocean acoustic fields,” M. B. Porter, J. Acoust. Soc. Am., Vol. 82, no. 4, pp. 1349-1359, October, 1987.
[10] “Computational Ocean Acoustics,” F. B. Jensen, W. A. Kuperman, M.B. Porter, and K. Schmidt, Springer-Verlag, New York: American Institute of Physics, 2000.

[11] "Robust Adaptive Beamforming," H. Cox, IEEE Trans. On Acoustics, Speech m and Signal Processing, vol. ASSP 35, pp. 1365-1376, Oct. 1987.
[12] "Robust adaptive matched-field processing," Y. Lee, H. Freese, J. Hanna, and P. Mikhalevsky, Proc. IEEE Oceans'93, vol.3, pp 387-392, October, 1993.

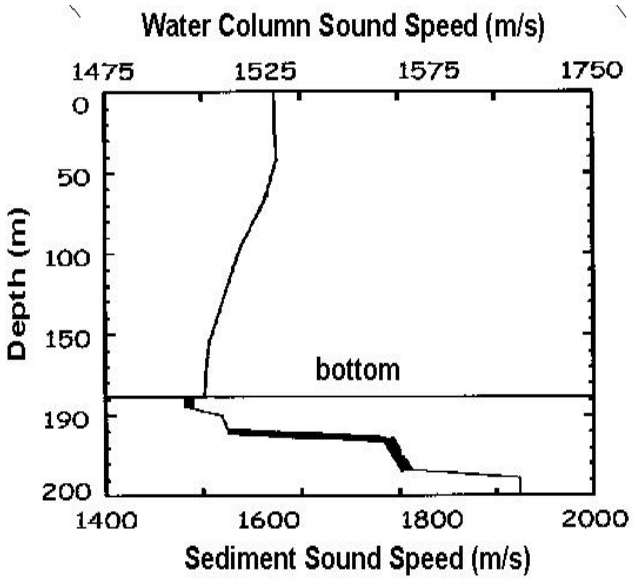

Figure 1: Measured sound speed profile in a Gulf of Mexico experiment.

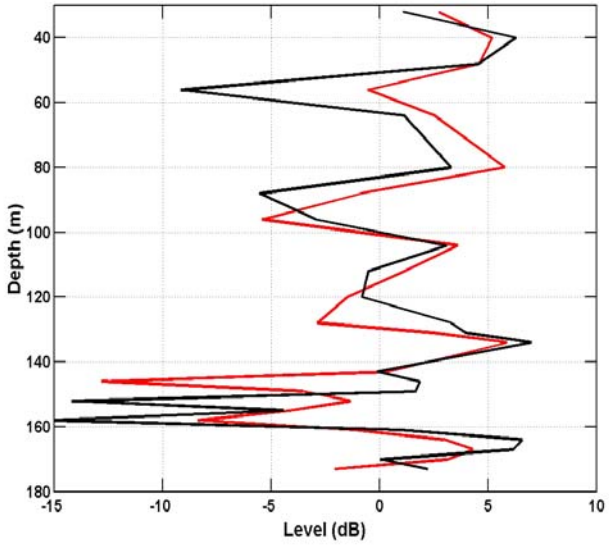

Figure 2: Measured (red) and predicted (black) pressure field for source at 9.06 km.

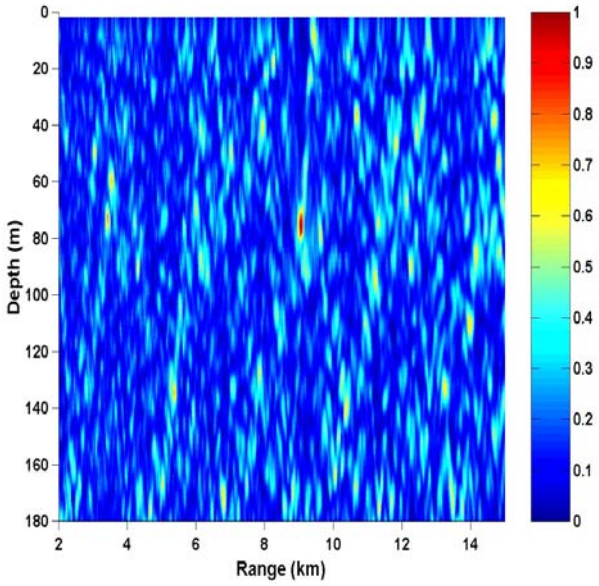

Figure 3: Conventional range-depth ambiguity surface with vertical array for a source at 9.06 km and depth of 76 m. The color scale is the cross correlation coefficient.

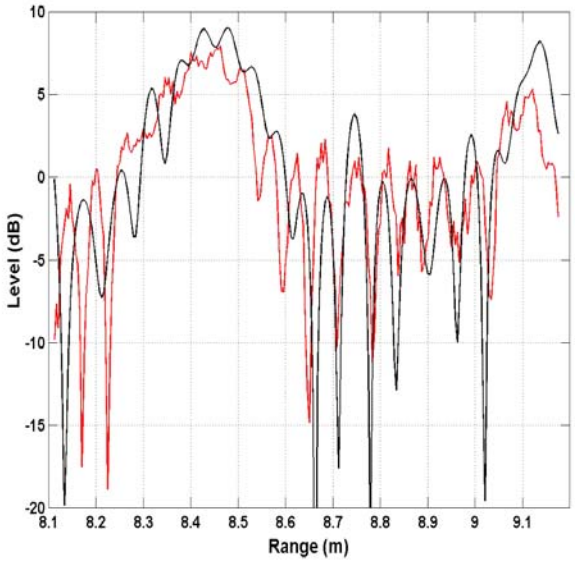

Figure 4: Measured (red) and predicted (black) pressure field on the bottom hydrophone for source towed at 2.5 m/s from 9.18 km toward the receiver.

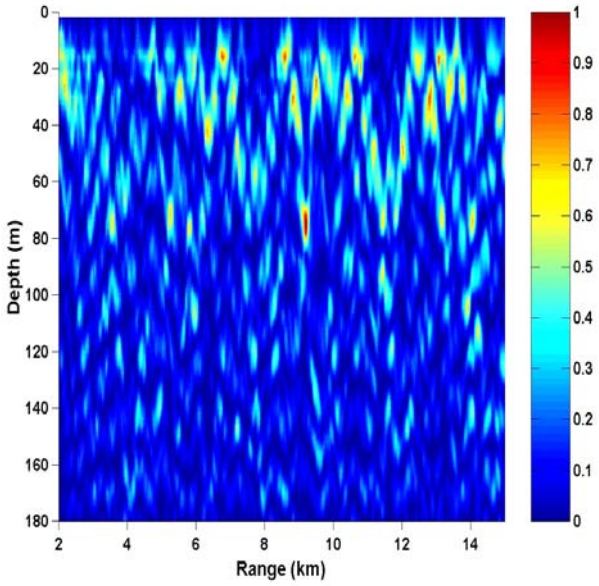

Figure 5: Conventional range-depth ambiguity surface of the single-element pre-Doppler MFP for source at 76 m towed at 2.5 m/s from 9.18 km. The color scale is the cross correlation coefficient.

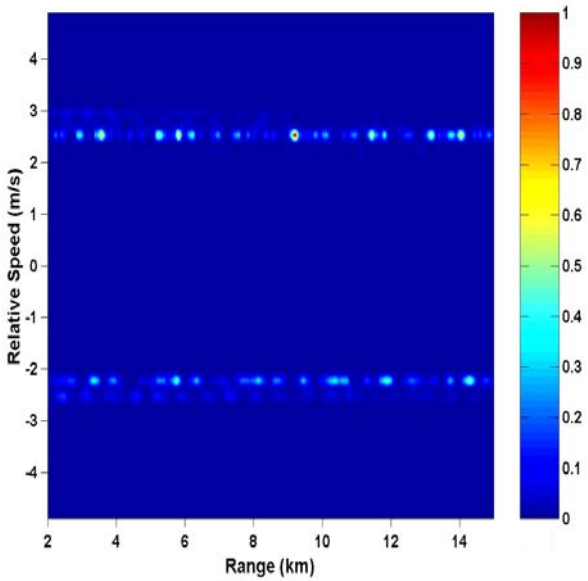

Figure 6: Conventional range-speed ambiguity surface of the single-element pre-Doppler MFP for source at 76 m towed at 2.5 m/s from 9.18 km. The color scale is the cross correlation coefficient.

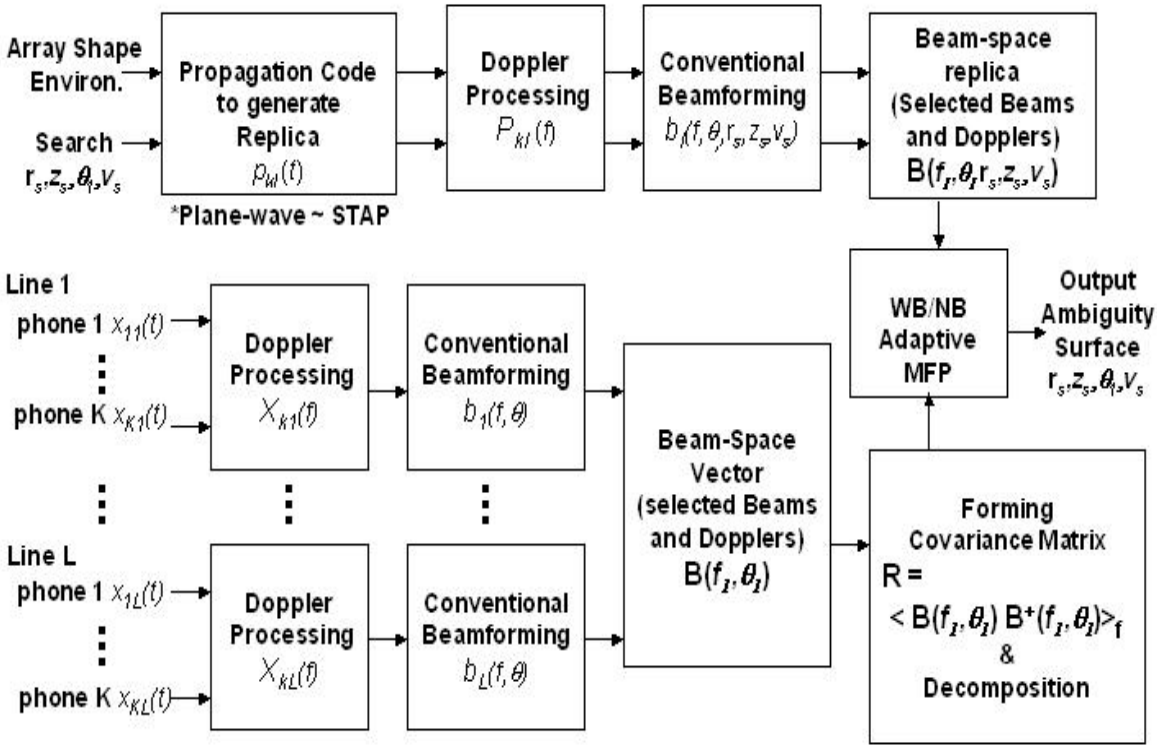

Figure 7: Space-Time Adaptive Matched-field Processing (STAMP)

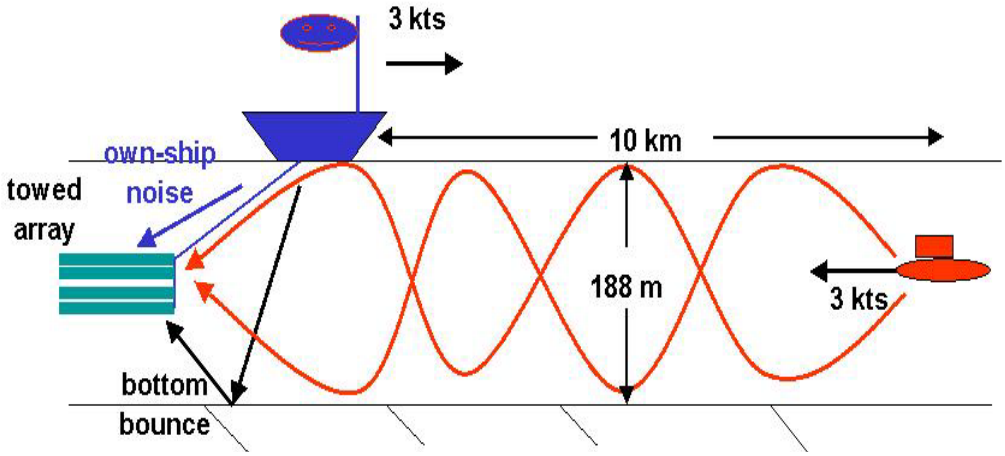

Figure 8: Forward sector simulation geometry, f=200 Hz, target(narrowband)=120 dB, own-ship(broadband)=120 dB, bottom bounce (broadband)=115 dB, white NL=120 dB, random phase error=0.1 wavelength, no environmental mismatch.

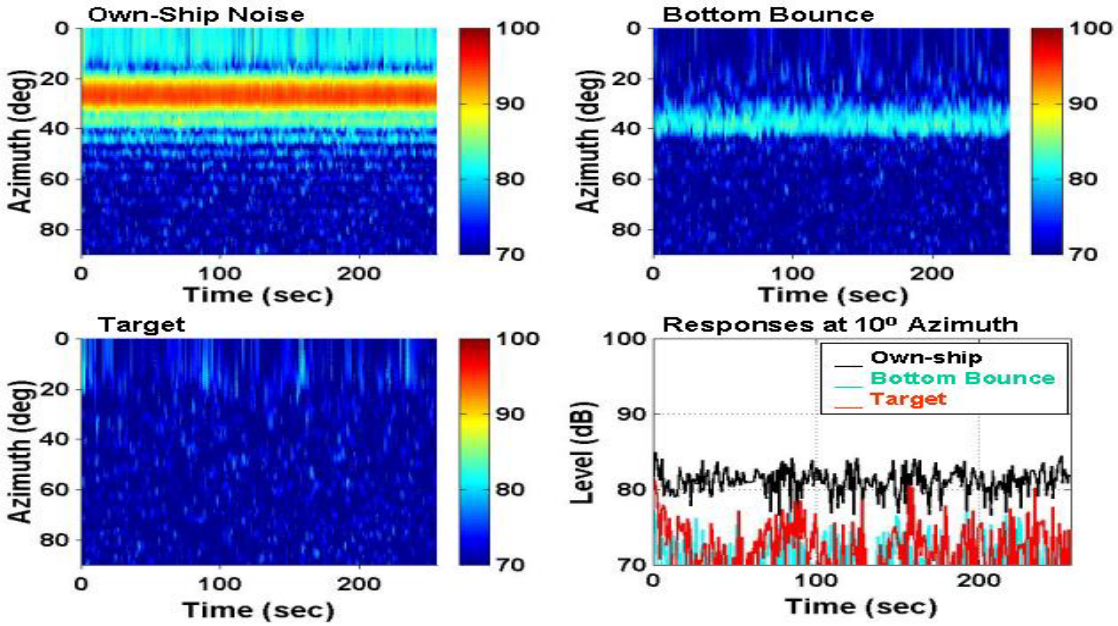

Figure 9: Single-Line BTRs of each signal component are shown in the top two and the bottom-left panels. The beam-time responses at 10o azimuth are shown in the bottom-right panel. The color scales are in dB.

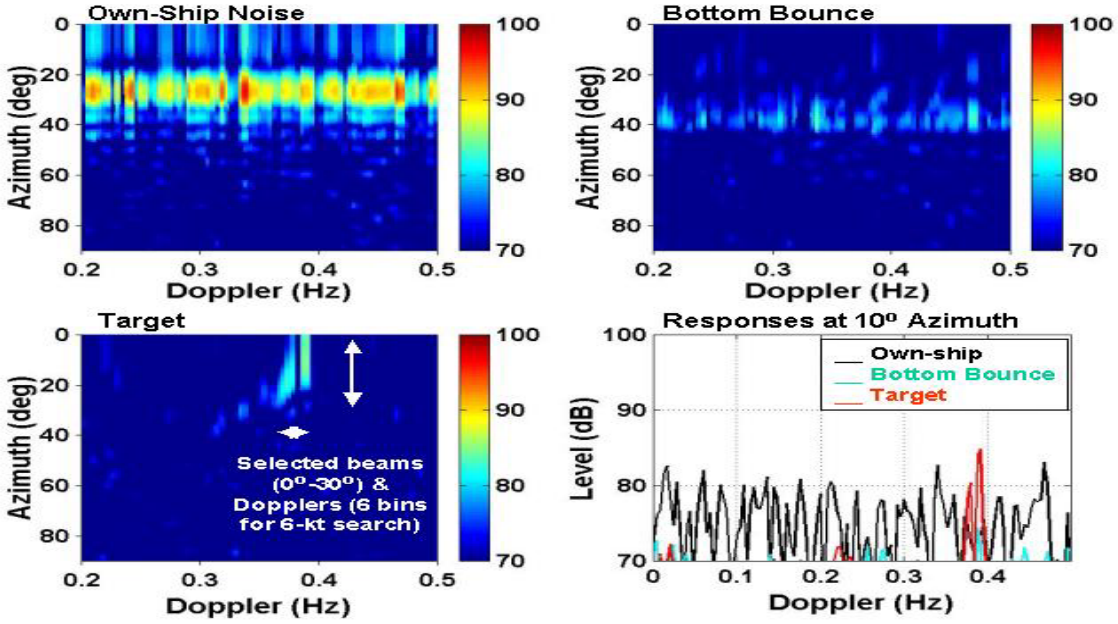

Figure 10: Single-Line Doppler/Azimuth responses with a 256-sec integration time of each signal component are shown in the top two and the bottom-left panels. The Doppler responses at 10° azimuth are shown in the bottom-right panel. The color scales are in dB.

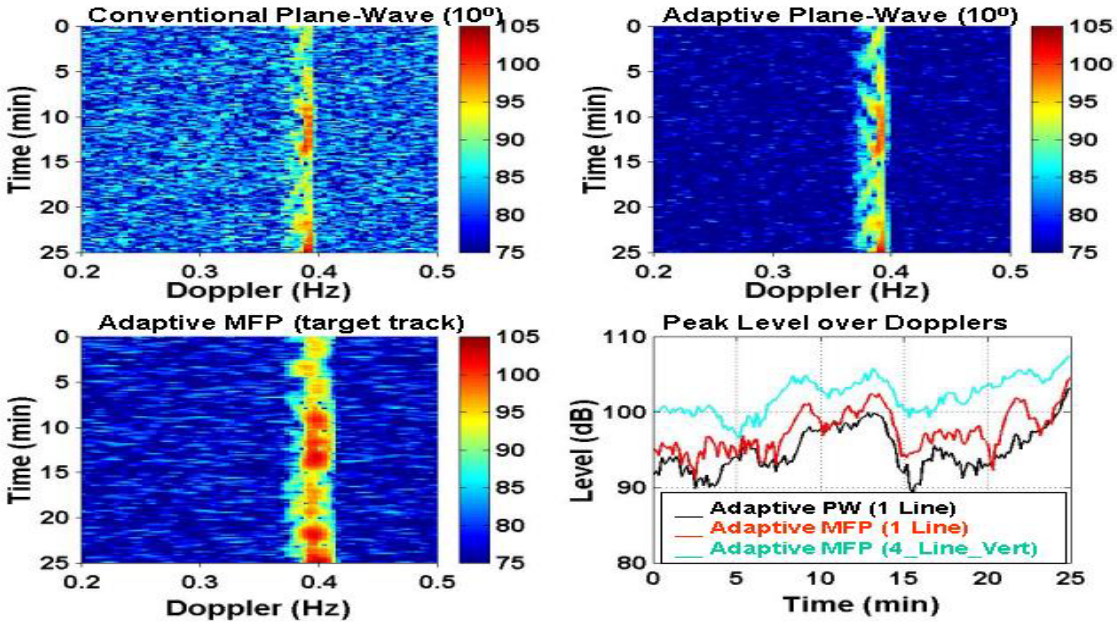

Figure 11: Single-Line spectrograms for the conventional and the adaptive plane-wave beamforming at 10° azimuth are shown in the top two panels. The single-line adaptive MFP track-cell spectrogram is shown in the bottom-left panel. The bottom-right panel shows the time histories of the peak responses over Doppler for single-line adaptive plane-wave beamforming, single-line adaptive MFP, and 4-vertical-line adaptive MFP. The color scales are in dB.

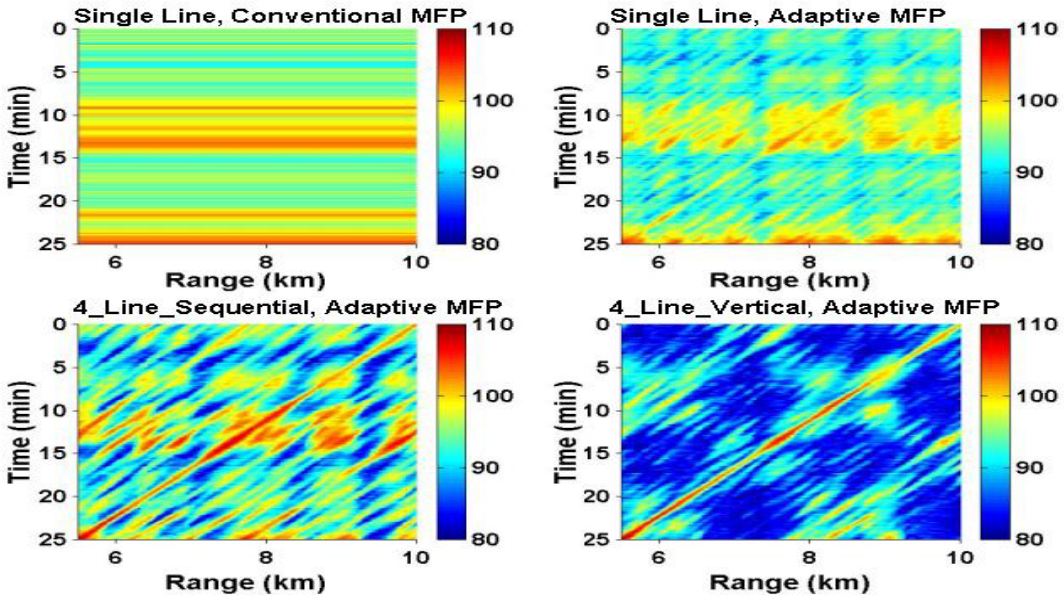

Figure 12: Array-size dependence of MFP range tracking at target depth and target speed. Target was from 10 km moving in to 6.5 km after 25 minutes. The top two panels show the track-cell-gram for the single-line conventional MFP and adaptive MFP. The bottom-left panel shows the 4-sequential-line adaptive MFP track-cell-gram. The bottom-right panel shows the 4-vertical-line adaptive MFP track-cell-gram. The color scales are in dB.

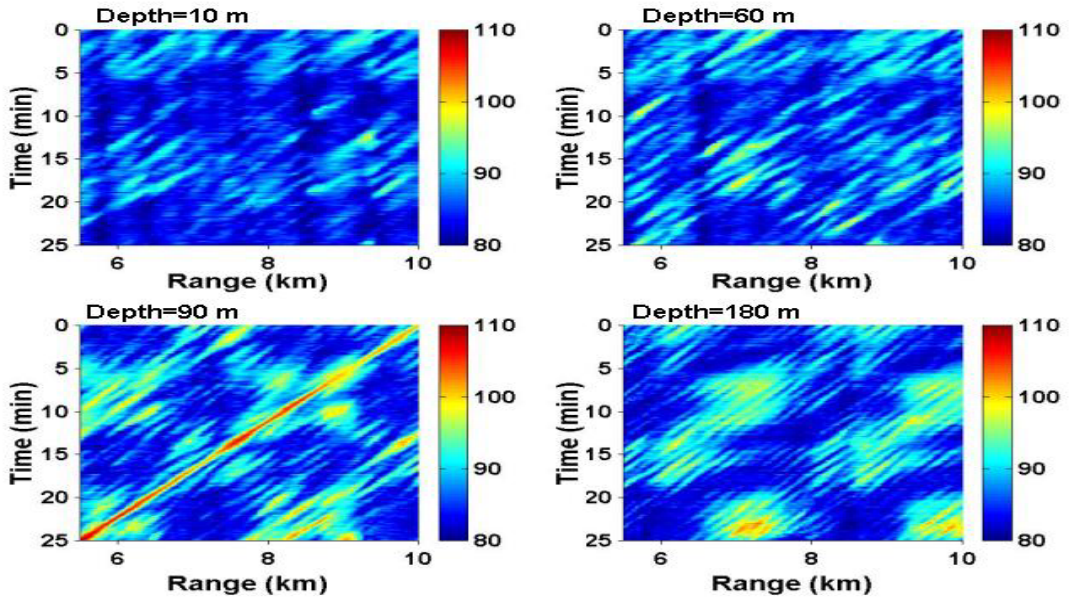

Figure 13: Depth discrimination of 4-vertical-line adaptive MFP range tracking at target speed. The top two panels show MFP track-cell-grams at depths of 10 m and 60 m. The bottom two panels show MFP track-cell-grams at depths of 90 m and 180 m. Target was at 90 m in depth and was from 10 km moving in to 6.5 km after 25 minutes. The color scales are in dB.

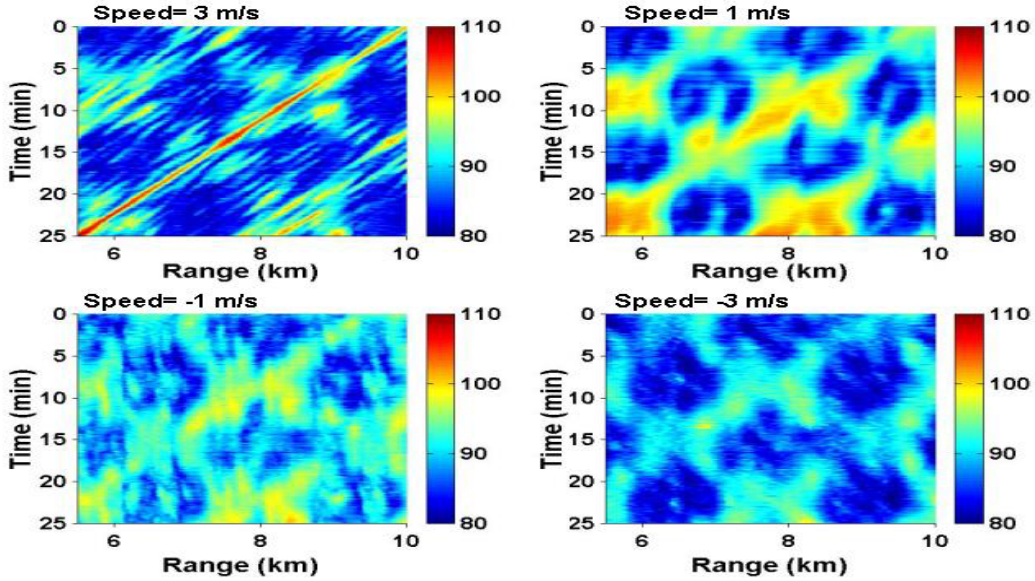

Figure 14: Speed discrimination of 4-vertical-line adaptive MFP range tracking at target depth. The top two panels show MFP track-cell-grams at speeds of 3 m/s and 1 m/s moving toward the array. The bottom two panels show MFP track-cell-grams at speeds of 1 m/s and 3 m/s moving away from the array. Target was moving toward the array at 3m/s and was from 10 km moving in to 6.5 km after 25 minutes. The color scales are in dB.